60-GHz Air Substrate Leaky-Wave Antenna Based on MEMS Micromachining Technology

Le Chang, *Student Member, IEEE*, Zhijun Zhang, *Fellow, IEEE*, Yue Li, *Member, IEEE*, Shaodong Wang, and Zhenghe Feng, *Fellow, IEEE*

***Abstract*— In this paper, a 60-GHz air substrate leaky-wave antenna based on microelectromechanical system (MEMS) bulk micromachining is proposed. Using penetration dry etching and gold plating processes, the air-filled leaky-wave slots, waveguide, and coupling slot, which are located in the top, middle, and bottom silicon-based layers, respectively, are generated. The three layers are stacked and clamped together using two location pins and five metal screws. The most distinctive feature of the proposed antenna is that the electromagnetic wave cannot see any substrates, except for the air medium, leading to good antenna performance. Good agreement between simulation and measurement demonstrates that the MEMS micromachining process fulfills the millimeter-wave (mm-wave) accuracy. To the best of the authors' knowledge, this is the first time that an air substrate mm-wave antenna is fabricated using the MEMS bulk micromachining technology. The fabricated prototype with a bandwidth of 17.3% and a peak gain of 11.4 dBi is attractive for mm-wave wireless communication applications. Validity of the feasibility provides the possibility to realize the system-in-package solutions.**

***Index Terms*— Antenna-in-package, dry etching, gold plating, leaky-wave antenna (LWA), microelectromechanical systems (MEMSs), micromachining, millimeter-wave (mm-wave), penetration etching, system-in-package (SiP).**

I. Introduction

With the increasing demand for faster data transmission and better system performance, the need to move up in frequency is necessary. The unlicensed 60-GHz frequency band has attracted much interest nowadays [1]–[12]. Millimeter-wave (mm-wave) communication around 60 GHz has the merits of frequency reuse and strong anti-interference performance. In addition, the 5-mm free-space wavelength makes the components and antennas easy to achieve miniaturization [6]. In this situation, mm-wave antennas have been a hotspot [6]–[12]. Subsequently, the challenge of precise machining arises. There are a lot of machining processes that can satisfy the mm-wave fabrication accuracy, such as microelectromechanical system (MEMS) micromachining, low temperature co-fired ceramic (LTCC), photoresist, and diffusion bonding technologies.

The term MEMS refers to microsystems that can integrate microsensors, microactuators, micropowers, signal processing and control circuits, and other components into a single chip [13]. Micromachining is the fundamental technology for fabricating MEMS components [14]. Silicon micromachining, which refers to fashioning a silicon-based substrate in the submillimeter range, is the most mature micromachining technology [15], [16]. This process is derived from IC processing technology that contains etching, diffusion, photoetching, ion injection, epitaxy, and vapor deposition processes. Silicon micromachining includes bulk micromachining and surface micromachining [13]. Bulk micromachining refers to fashioning the bulk of single-crystal silicon wafers by selectively removing the wafer portions. It was first adopted to fabricate antennas in 1998 [17]. Since then, mm-wave antennas started to be fabricated by means of this technique [18], [19]. The thicknesses of the realized microstructures using bulk micromachining cover the range from submicrometer to full wafer thickness (200–500 μm) and the longitudinal accuracy is at the submicrometer level as well. Nowadays, the majority of MEMS devices are manufactured using bulk micromachining. Surface micromachining does not manipulate the bulk silicon but instead builds structures on the surface of the silicon by depositing thin films of "sacrificial layers" and "structural layers," and then etching off the sacrificial layers to form the ultimate mechanical microstructures [20]–[21]. However, the process sequence is complex, the device assembly is difficult, and the ultimate microstructures are usually planar structures, not real 3-D [13]. LIGA, which is a German acronym with an English translation of lithography, electroforming, and molding, belongs to MEMS microfabrication. Antennas fabricated using LIGA process have high aspect ratio as much as 200, and the verticality of the sidewalls is higher than 89.9° [22], [23]. However, the high cost of X-ray lithography limits the application of LIGA, and it is difficult to be integrated with IC [13]. LTCC is the mainstream multilayer substrates packaging integrated technology, especially beneficial for high-frequency applications [24], [25]. It has been widely used to fabricate mm-wave antenna arrays [6]–[8]. However, structures with too many layers make the design complex. NASA's Jet Propulsion Laboratory has fabricated

Manuscript received May 31, 2016; revised September 12, 2016; accepted October 9, 2016. Date of publication October 28, 2016; date of current version November 7, 2016. This work was supported in part by the National Basic Research Program of China under Contract 2013CB329002, in part by the National Natural Science Foundation of China under Contract 61371012 and Contract 61525104, and in part by the China Postdoctoral Science Foundation Funded Project under Grant 2015T80084. Recommended for publication by Associate Editor W.-Y. Yin upon evaluation of reviewers' comments.

L. Chang, Z. Zhang, Y. Li, and Z. Feng are with the State Key Laboratory on Microwave and Communications and the Tsinghua National Laboratory for Information Science and Technology, Tsinghua University, Beijing 100084, China (e-mail: zjzh@tsinghua.edu.cn).

S. Wang is with the Hebei Semiconductor Research Institute, Shijiazhuang 050000, China.

Color versions of one or more of the figures in this paper are available online at http://ieeexplore.ieee.org.

Digital Object Identifier 10.1109/TCPMT.2016.2616516

numerous sub-mm-wave components using the photoresist process [26], [27]. SU-8 photoresist process is an important branch, and it is especially applicable for manufacturing relatively thick (hundreds of micrometers) microstructures with nearly vertical sidewalls [28]. Antennas or filters manufactured using SU-8 photoresist technology usually have a high aspect ratio (50:1), and the longitudinal fabrication precision is as high as the micrometer level, resulting in terahertz operation [29], [30]. However, it is difficult to control the flatness and homogeneity of the photoresist; thus, the thickness accuracy is relatively insufficient. Diffusion bonding is a solid-state welding technique based on the atom diffusion migration principle, capable of joining similar and dissimilar metals, and reactive and refactory metals [31]. A lot of work has been involved in mm-wave slot arrays in this area [9], [10]. However, this technology is difficult to realize mass production, owing to the rigorous demand for the abutting surfaces and the long clamping time. Substrate integrated waveguide (SIW) structures are another solution for mm-wave antennas. Conventional/flexible printed circuit board (PCB) techniques [32], [33], LTCC [7], and photoimageable thick-film technologies [34] are some implementation approaches to realize SIW antennas or filters. However, the dielectric loss is a severe issue at mm-waveband, especially when the SIW array dimension becomes large [32]. In addition, the metalized via holes complicate the manufacturing process.

On the other hand, the new trend in the mm-wave antenna design is turning from the traditional discrete designs to antenna-in-package solutions, considering the system-in-package (SiP) architectures requirement, which pursues the integration of the RF frontend and signal processing circuit on a single chip-scale package [35], [36]. LTCC can accomplish this kind of integration; however, it is incompatible with the silicon semiconductor substrate. Other technologies abovementioned cannot be used to manipulate the silicon wafer except for the MEMS microchining process. In addition, the signal processing circuit can be fabricated on the silicon wafer. Thus, the SiP solutions may be realized at a relatively low cost using the MEMS micromachining technology.

In this paper, the feasibility of fabricating a 60-GHz high-performance antenna using the MEMS bulk micromachining technology is explored. As is well known, the silicon substrate is not suitable to design antennas directly due to its high dielectric constant. Herein, the penetration etching process is adopted to fabricate 60-GHz air substrate leaky-wave antennas (LWAs). LWAs originated from a slotted waveguide in the 1940s [37]. Since then, LWAs based on microstrip line [38], SIW [39], parallel-plate waveguide [40], and composite right/left-handed [41] have been developed rapidly. An overview of LWAs is detailed in [42]. LWAs can be fed from one end to acquire scanning beam [38] or at the center to achieve broadside beam [40]. In this paper, the antenna consists of three silicon-based layers: the top layer with four leaky-wave slots, the middle layer with the air rectangular waveguide, and the bottom layer with the coupling slot. The three silicon layers are stacked and clamped together using two location pins and five screws. The 410 series waveguide-to-coax transition [43] is used for feeding the proposed antenna. The energy is leaked out through the four slots, constituting a leaky-wave waveguide antenna. All the air cavities are fabricated using penetration dry etching and gold-plating processes. To the best of the authors' knowledge, this is the first time that a mm-wave antenna is realized using the MEMS bulk micromachining technology, making the proposed antenna filled with air substrate only, without any substrates. The measured impedance bandwidth of the fabricated prototype is 17.3%. The radiation patterns in the whole operating band are stable, and the peak gain is 11.4 dBi. Validity of the feasibility provides the possibility to realize the SiP solutions.

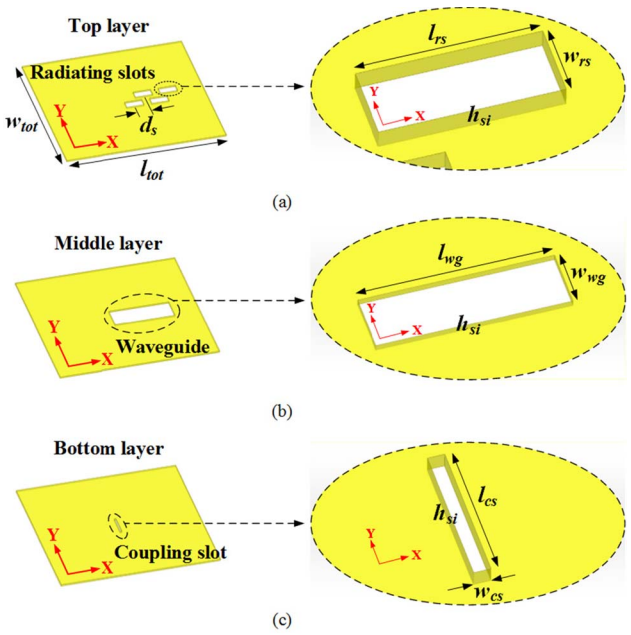

Fig. 1. (a) Top layer. (b) Middle layer. (c) Bottom layer. Left column: exploded view of the proposed antenna. Right column: detailed illustrations of the radiating slots, waveguide, and coupling slot.

II. Antenna Geometry

A. Antenna Geometry

Fig. 1 shows the exploded view of the proposed antenna (left column) and a detailed illustration of the penetration structures (right column). The commercial 3-D electromagnetic field solver HFSS version 14 is used to design and optimize the proposed antenna. In our design, the silicon substates are single-crystal silicon wafers with a permittivity of 11.9. The air-filled radiating slots, air rectangular waveguide, and coupling slot are fabricated using penetration dry etching and gold-plating processes based on MEMS bulk micromachining technology. The four radiating slots and waveguide are located in the right portions of their respective substrates. The rightmost slot's rightmost wall aligns with the waveguide's rightmost wall. The energy is coupled from the standard 60-GHz waveguide (WR15) to the air rectangular waveguide. The coupling slot lying between the WR15 and the rectangular waveguide is used to adjust impedance matching: dimension of the coupling slot, and the distance between the slot and the waveguide's leftmost wall are the degrees of freedom.

TABLE I
DETAILED DIMENSIONS OF THE PROPOSED ANTENNA (mm)

Parameter	l_{tot}	w_{tot}	h_{si}	l_{cs}	w_{cs}
Value	32	25	0.4	3.4	0.4
Parameter	l_{wg}	w_{wg}	l_{rs}	w_{rs}	d_s
Value	12	3.6	3.5	1.4	2.5

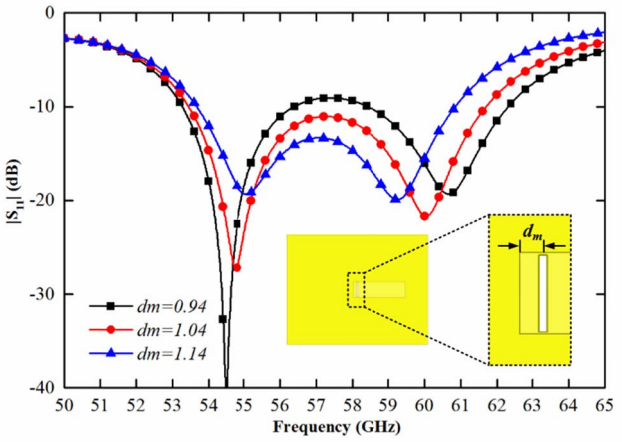

Fig. 2. Magnitude of reflection coefficients with variation of d_m (mm). The enlarged view of the inset illustrates the distance d_m.

The detailed dimensions of the silicon substrate layers and the three types of penetration structures are shown in the right column of Table I. All the silicon substrates share the common total dimensions ($l_{\text{tot}} \times w_{\text{tot}} \times h_{\text{si}}$) of $32 \times 25 \times 0.4$ mm^3. The sidewall verticality of these penetration structures is 88°, not perfectly plumb. These tilts have been considered in simulation, although they hardly affect the antenna performance. The dimensions in the horizontal plane of these penetration structures refer to the dimensions at the bottom, and they are slightly larger than that of the top. The four slots share the same dimensions ($l_{\text{rs}} \times w_{\text{rs}}$) of 3.5×1.4 mm^2, and the element spacing (d_s) is 2.5 mm. The dimensions of the waveguide ($l_{\text{wg}} \times w_{\text{wg}}$) and coupling slot ($l_{\text{cs}} \times w_{\text{cs}}$) are 12×3.6 mm^2 and 3.4×0.4 mm^2, respectively.

The relative position between the coupling slot and the rectangular waveguide is indicated by the distance (d_m) between the coupling slot and the leftmost wall of the waveguide. It is shown in the enlarged figure in the inset of Fig. 2, and it is a crucial parameter for impedance matching. The magnitude of reflection coefficients under different distances are given in Fig. 2. When the distance is equal to 1.14 mm, the bandwidth is narrow, and when it is equal to 0.94 mm, some frequency points in the middle band are higher than -10 dB. Finally, the optimized value of 1.04 mm is selected. The optimized value indicates that the energy coupled from the coupling slot to the waveguide flows to the leakage slots for radiating with slight reflection.

In the assembling process, the three silicon layers are clamped together with the penetration structures' bigger openings orientated at the bottom using two location pins and five metal screws. The location holes reserved for pins and screws are not illustrated in the geometry for brevity.

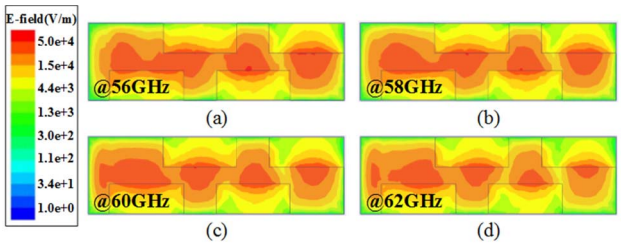

Fig. 3. Aperture electric field distributions at (a) 56, (b) 58, (c) 60, and (d) 62 GHz.

The 410 series waveguide-to-coax transition is used for testing the proposed antenna. The center of the testing waveguide with a dimension of 3.759×1.88 mm^2 aligns with that of the coupling slot. In simulation, a wave port is attached to a 2-mm-long air waveguide whose dimension is the same as the realistic feeding waveguide.

B. Leaky-Wave Antenna

The width of the air rectangular waveguide is selected to be approximately $0.7\lambda_0$, which is the typical value of the conventional waveguide width [44]. The dimensions of the radiating slots are $0.7\lambda_0 \times 0.28\lambda_0$, which is larger than the conventional waveguide slots. The reason for this is that effective radiation can be achieved within a relatively small longitudinal size.

The aperture electric field distributions at four different frequencies are depicted in Fig. 3. As seen, at these four frequencies, except for the rightmost slot, there is no clear null in the rest of the three slots. This indicates that the traveling wave exists in the first three slots, and the wave is traveling while leaked out into free space for effective radiation.

III. MEMS MICROMACHINING PROCESS AND THE MEASURED RESULTS

A. MEMS Micromachining Process

A prototype of the proposed antenna is fabricated and measured to verify the proposed design. The photographs of the three silicon substrate layers, the 410 series waveguide-to-coax transition, and the whole antenna are depicted in Fig. 4(a)–(c). A 2-mm-thick copper plate shown in Fig. 4(a) connects the feeding waveguide and the three silicon substrate layers. The dimension of the air waveguide in the plate is the same as the feeding waveguide. Another function of the copper plate layer is to protect the three fragile silicon substrate layers and clamp them together tightly.

The fabrication process is based on MEMS bulk micromachining technology. In the first step, the penetration structures and location holes are etched away using dry etching with sulfur hexafluoride gas. Etching ensures a high precision of about ± 4 μm. Limited by the dry etching process, the sidewall verticality of these penetration structures is not perfectly plumb, as shown in the inset of Fig. 4(a). The enlarged photograph is taken on the left side of the AA′-cut with the help of a Nikon SMZ745 microscope. As seen, the sidewalls

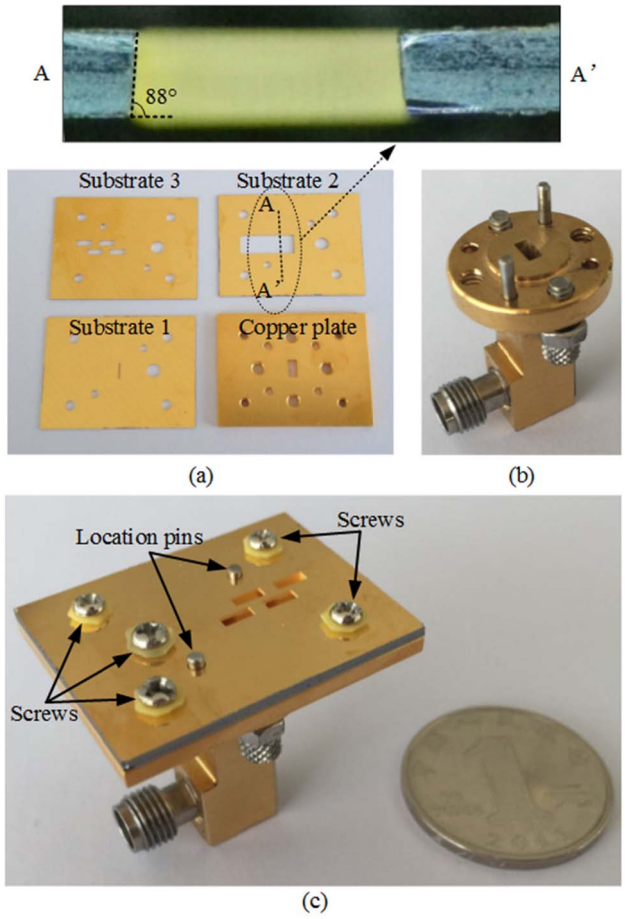

Fig. 4. Photographs of the fabricated 60-GHz air substrate LWA. (a) Top view of the silicon substrates and copper plate. (b) 410 series waveguide-to-coax transition for testing. (c) Whole antenna.

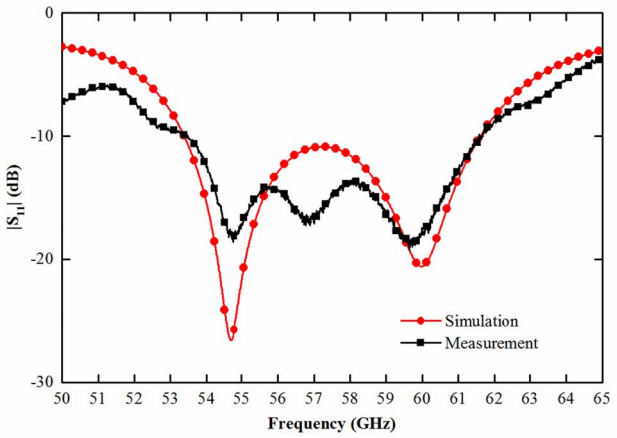

Fig. 5. Simulated and measured magnitudes of reflection coefficients of the proposed antenna.

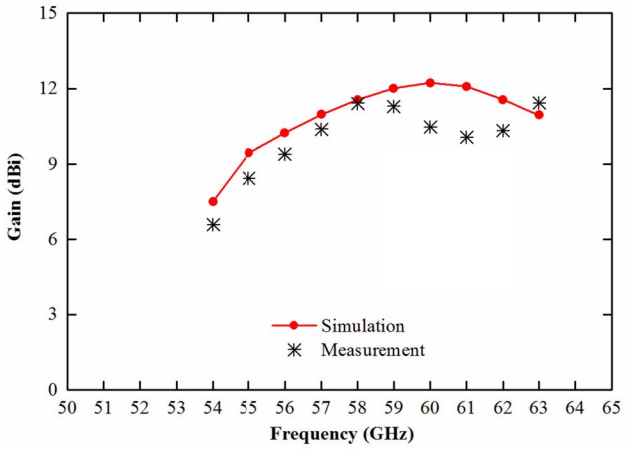

Fig. 6. Simulated and measured broadside gains of the proposed antenna.

have a tilt angle of 88°. However, these tilts hardly affect the antenna performance. Then, all the faces and sidewalls are gold-plated. The thickness of the gold layers is 3.5 μm with a tolerance of ± 0.5 μm. Finally, the assembling process is conducted manually. As mentioned above, these penetration structures' bigger openings are orientated at the bottom. All the layers are clamped together using location pins and screws. The measured total thickness of the three layers in addition to the copper plate is 3220 ± 20 μm, which is very close to the ideal value of 3221 μm.

As for the traditional PCB technique, the milling process is used to fabricate these air cavities. However, usually the fabrication tolerance is larger than 100 μm, leading to an unreliable antenna performance in mm-waveband. The fabrication tolerance of the etching and gold-plated processes based on MEMS micromachining technology is far beyond that of the traditional PCB technique. Therefore, mm-wave antennas fabricated using the MEMS technique have a reliable and repeatable performance.

B. Impedance Bandwidth, Gain, and Radiation Patterns

Reflection coefficient, gain, and radiation patterns are measured using an N5247A vector network analyzer (10 MHz–67 GHz). The gain is obtained by gain comparison method with a standard horn as a reference.

The simulated and measured magnitude of reflection coefficients are shown in Fig. 5. The simulated bandwidth is 14.3% from 53.4 to 61.6 GHz, while the measured bandwidth is 17.3% from 52.8 to 62.8 GHz for $|S_{11}| < -10$ dB. They agree well with each other.

Fig. 6 shows the simulated and measured broadside gains. In simulation, the gain increases with the increase of frequency when the frequency is below 60 GHz, and the gain reaches its maximum of 12.2 dBi at 60 GHz. The gain has a small decrease when the frequency is higher than 60 GHz. The measured gain curve fits the simulated one. The maximum gain is 11.4 dBi at 58 GHz, the measured gains are a little lower than simulation, and a slight discrepancy happens between 60 and 62 GHz. The measured 3-dB gain bandwidth is 13.24% from 55 to 62.8 GHz, which is the same as the simulation. The deviation between simulation and measurement is caused by assembly and measurement errors.

Fig. 7 shows the simulated and measured radiation patterns in two principal planes at 54, 57, and 60 GHz, respectively. The backward radiation is not measured due to the rather

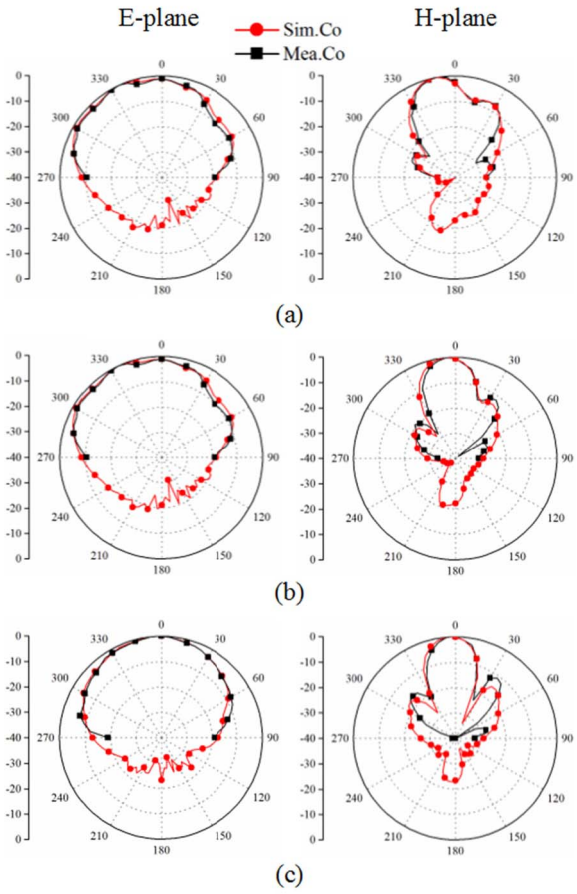

Fig. 7. Simulated and measured radiation patterns of the proposed antenna at (a) 54, (b) 57, and (c) 60 GHz.

TABLE II
SIMULATED AND MEASURED 3-dB BEAMWIDTHS

Frequency (GHz)	E-plane		H-plane	
	Simulated	Measured	Simulated	Measured
54	81°	85°	25°	25°
57	86°	85°	27°	25°
60	70°	70°	25°	25°

weak back lobe levels (approximately lower than −20 dB). Fan-shaped beams are observed, and the simulated and measured forward radiation patterns in both E-plane (yz-plane) and H-plane (xz-plane) are in good agreement. When the operating frequency decreases, the maximum directions deviate from the broadside further. The maximum directions at 54, 57, and 60 GHz have tilt angles of 12°, 6°, and 3° respectively. Beam scanning is a typical feature of the LWA. The slight discrepancy is caused by assembly and measurement errors. The simulated and measured 3-dB beamwidths in both the E- and H-plane at 54, 57, and 60 GHz are listed in Table II. The measurement agrees well with the simulation, and the 3-dB beamwidths are stable throughout the frequency band.

Therefore, the proposed 60-GHz LWA has the merits of low loss, relatively broad bandwidth, stable radiation patterns, and gains. Good agreement between simulation and measurement validates that the fabrication tolerance is sufficient for mm-wave applications. If the input interface is converted from the waveguide-to-coax transition to waveguide-to-GSG (ground-signal-ground) transition, the antenna can be integrated with the signal processing circuit, so the SiP solutions can be satisfied.

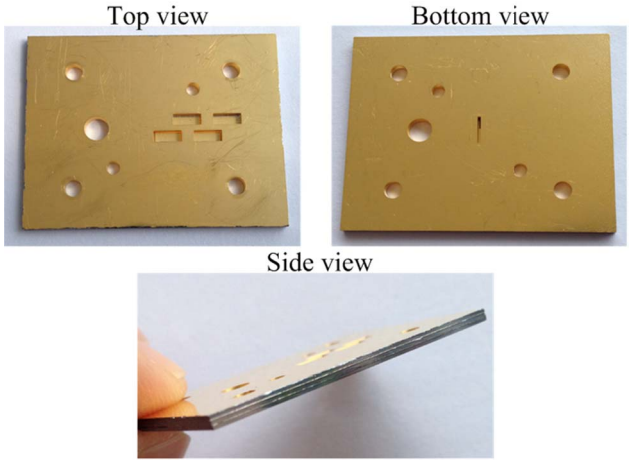

Fig. 8. Photographs of the antenna assembled by intermediate layer-assisted bonding technique.

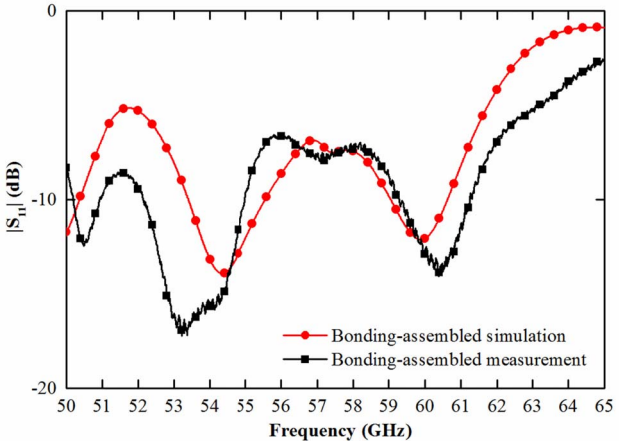

Fig. 9. Simulated and measured magnitude of reflection coefficients of the bonding-assembled antenna.

C. Intermediate Layer Assisted Bonding

Another assembly technique called the intermediate layer-assisted bonding can be used to assemble the multiple layers as well. It refers to the three silicon layers joined together with the help of the 50-μm-thick AuSn solder. Two AuSn solder layers are sandwiched in the three silicon layers and then are stacked and aligned in the specific fixture. Next, they are put into the vacuum sintering furnace for firing by applying a temperature of approximately 300 °C. After about only 30 s, the three silicon-based layers are bonded into a whole. Finally, the whole structure and the copper plate are clamped together using the location pins and screws. The antenna prototype assembled using intermediate layer assisted bonding is shown in Fig. 8, and the measured magnitude of reflection coefficient is shown in Fig. 9. The antenna assembled by this bonding technique loses the

original relative broadband performance, impedance matching in the middle frequency band from 50.93 to 52.14 GHz gets worse, and the bandwidth splits into a dual band. The deviation stems from two aspects. First, the two solder layers thicken the middle silicon layer. The measured thickness of the three bonding layers is 1329 ± 20 μm compared to the ideal value of 1221 μm. Consequently, the height of the air-filled waveguide is increased, leading to mismatch. Second, after elaborately watching the bonded structure with a microscope, the bottom and middle layers bonded well, whereas an air gap is observed between the top and the middle layers. Based on the above analysis, 100-μm thickening of the middle silicon layer and two identical air gaps of the same volume as $17 \times 1.53 \times 0.05$ mm^3 next to the air-filled transmission line between the top and middle layers are assumed for simulation. The simulated result is depicted in Fig. 9. The simulated and measured results show a similar trend. Therefore, if the antenna is assembled using the intermediate-layer AuSn-assisted bonding technology, on one band, a 100-μm thickening of the middle silicon layer should be considered in advance before designing. On the other hand, we will explore the bonding technology further, and an ideal electrical interconnection of all the layers without any air gaps is expected. We plan to solve this issue in the near future.

IV. Conclusion

A new fabrication technique based on MEMS bulk micromachining technology is proposed to fabricate the air substrate mm-wave antenna for the first time. The antenna with three silicon-based layers is fabricated using penetration dry etching and gold-plating processes. All the layers are stacked and fixed together using location pins and screws. The electromagnetic wave is only interacted with air medium, leading to good antenna performance. A prototype with a measured impedance bandwidth of 17.3%, a broadside gain up to 11.4 dBi, and a 3-dB gain bandwidth of 13.56% is fabricated and measured to verify the design strategy and that the MEMS micromachining process is suitable for fabricating mm-wave antennas. Moreover, the SiP solutions can be fulfilled by altering the input interface. We have confirmed this point, and the SiP product has already been available. In the future, we will focus on terahertz applications to further explore the limit fabrication tolerance of the MEMS micromachining process.

References

[1] P. Smulders, "Exploiting the 60 GHz band for local wireless multimedia access: Prospects and future directions," *IEEE Commun. Mag.*, vol. 40, no. 1, pp. 140–147, Jan. 2002.

[2] H.-H. Yeh and K. L. Melde, "Development of 60-GHz wireless interconnects for interchip data transmission," *IEEE Trans. Compon., Packag., Manuf. Technol.*, vol. 3, no. 11, pp. 1946–1952, Nov. 2013.

[3] S. R. Aroor and R. M. Henderson, "Loss performance of planar interconnects on FR-4 up to 67 GHz," *IEEE Trans. Compon., Packag., Manuf. Technol.*, vol. 3, no. 12, pp. 2127–2133, Dec. 2013.

[4] S. Seok and J. Kim, "Design, fabrication, and characterization of a wideband 60 GHz bandpass filter based on a flexible PerMX polymer substrate," *IEEE Trans. Compon., Packag., Manuf. Technol.*, vol. 3, no. 8, pp. 1384–1389, Aug. 2013.

[5] I. Haroun, C. Plett, Y.-C. Hsu, and D.-C. Chang, "Compact 60-GHz IPD-based branch-line coupler for system-on-package V-band radios," *IEEE Trans. Compon., Packag., Manuf. Technol.*, vol. 2, no. 7, pp. 1070–1074, Jul. 2012.

[6] L. Wang, Y. X. Guo, and W. X. Sheng, "Wideband high-gain 60-GHz LTCC L-probe patch antenna array with a soft surface," *IEEE Trans. Antennas Propag.*, vol. 61, no. 4, pp. 1802–1809, Apr. 2013.

[7] Y. Li, Z. N. Chen, X. Qing, Z. Zhang, J. Xu, and Z. Feng, "Axial ratio bandwidth enhancement of 60-GHz substrate integrated waveguide-fed circularly polarized LTCC antenna array," *IEEE Trans. Antennas Propag.*, vol. 60, no. 10, pp. 4619–4626, Oct. 2012.

[8] A. E. I. Lamminen, J. Saily, and A. R. Vimpari, "60-GHz patch antennas and arrays on LTCC with embedded-cavity substrates," *IEEE Trans. Antennas Propag.*, vol. 56, no. 9, pp. 2865–2874, Sep. 2008.

[9] Y. Miura, J. Hirokawa, M. Ando, Y. Shibuya, and G. Yoshida, "Double-layer full-corporate-feed hollow-waveguide slot array antenna in the 60-GHz band," *IEEE Trans. Antennas Propag.*, vol. 59, no. 8, pp. 2844–2851, Aug. 2011.

[10] M. Zhang, J. Hirokawa, and M. Ando, "An E-band partially corporate feed uniform slot array with laminated quasi double-layer waveguide and virtual PMC terminations," *IEEE Trans. Antennas Propag.*, vol. 59, no. 5, pp. 1521–1527, May 2011.

[11] D. G. Kam, D. Liu, A. Natarajan, S. K. Reynolds, and B. A. Floyd, "Organic packages with embedded phased-array antennas for 60-GHz wireless chipsets," *IEEE Trans. Compon., Packag., Manuf. Technol.*, vol. 1, no. 11, pp. 1806–1814, Nov. 2011.

[12] B. Zhang, D. Titz, F. Ferrero, C. Luxey, and Y. P. Zhang, "Integration of quadruple linearly-polarized microstrip grid array antennas for 60-GHz antenna-in-package applications," *IEEE Trans. Compon., Packag., Manuf. Technol.*, vol. 3, no. 8, pp. 1293–1300, Aug. 2013.

[13] V. K. Varadan, K. J. Vinoy, and K. A. Jose, *RF MEMS and Their Applications*. 2nd ed. New York, NY, USA: Wiley, 2003.

[14] T. A. Baginski, R. N. Dean, and E. J. Wild, "Micromachined planar triggered spark gap switch," *IEEE Trans. Compon., Packag., Manuf. Technol.*, vol. 1, no. 9, pp. 1480–1485, Sep. 2011.

[15] M. Beiley, J. Leung, and S. S. Wong, "A micromachined array probe card-fabrication process," *IEEE Trans. Compon., Packag., Manuf. Technol. B*, vol. 18, no. 1, pp. 179–183, Feb. 1995.

[16] M. Beiley, J. Leung, and S. S. Wong, "A micromachined array probe card-characterization," *IEEE Trans. Compon., Packag., Manuf. Technol., B*, vol. 18, no. 1, pp. 184–191, Feb. 1995.

[17] I. Papapolymerou, R. F. Drayton, and L. P. B. Katehi, "Micromachined patch antennas," *IEEE Trans. Antennas Propag.*, vol. 46, no. 2, pp. 275–283, Feb. 1998.

[18] G. P. Gauthier, J. P. Raskin, L. P. B. Katehi, and G. M. Rebeiz, "A 94-GHz aperture-coupled micromachined microstrip antenna," *IEEE Trans. Antennas Propag.*, vol. 47, no. 12, pp. 1761–1766, Dec. 1999.

[19] G. M. Rebeiz, D. P. Kasilingam, Y. Guo, P. A. Stimson, and D. B. Rutledge, "Monolithic millimeter-wave two-dimensional horn imaging arrays," *IEEE Trans. Antennas Propag.*, vol. 38, no. 9, pp. 1473–1482, Sep. 1990.

[20] Y.-J. Kim and M. G. Allen, "Surface micromachined solenoid inductors for high frequency applications," *IEEE Trans. Compon., Packag., Manuf. Technol. C*, vol. 21, no. 1, pp. 26–33, Jan. 1998.

[21] B. Pan, Y.-K. Yoon, G. E. Ponchak, M. G. Allen, J. Papapolymerou, and M. M. Tentzeris, "Analysis and characterization of a high-performance Ka-band surface micromachined elevated patch antenna," *IEEE Antennas Wireless Propag. Lett.*, vol. 5, pp. 511–514, 2006.

[22] S. S. Gearhart and T. Willke, "Integrated antennas and filters fabricated using micromachining techniques," in *Proc. IEEE Aerosp. Conf.*, vol. 3. Mar. 1998, pp. 249–254.

[23] T. L. Willke and S. S. Gearhart, "LIGA micromachined planar transmission lines and filters," *IEEE Trans. Microw. Theory Techn.*, vol. 45, no. 10, pp. 1681–1688, Oct. 1997.

[24] R. R. Tummala *et al.*, "The SOP for miniaturized, mixed-signal computing, communication, and consumer systems of the next decade," *IEEE Trans. Adv. Packag.*, vol. 27, no. 2, pp. 250–267, May 2004.

[25] K.-S. Chin, C.-C. Chang, C.-H. Chen, Z. Guo, D. Wang, and W. Che, "LTCC multilayered substrate-integrated waveguide filter with enhanced frequency selectivity for system-in-package applications," *IEEE Trans. Compon., Packag., Manuf. Technol.*, vol. 4, no. 4, pp. 664–672, Apr. 2014.

[26] C. Jung-Kubiak *et al.*, "Silicon microfabrication technologies for THz applications," in *Proc. IEEE Silicon Nanoelectron. Workshop (SNW)*, Jun. 2012, pp. 1–2.

[27] N. Llombart *et al.*, "Silicon micromachined lens antenna for THz integrated heterodyne arrays," *IEEE Trans. Terahertz Sci. Technol.*, vol. 3, no. 5, pp. 515–523, Sep. 2013.

[28] *SU-8 Photoresist*, accessed on Sep. 7, 2016. [Online]. Available: https://en.wikipedia.org/wiki/SU-8_photoresist

[29] X. C. Wang, W. S. Zhao, J. Hu, and W. Y. Yin, "Reconfigurable terahertz leaky-wave antenna using graphene-based high-impedance surface," *IEEE Trans. Nanotechnol.*, vol. 14, no. 1, pp. 62–69, Jan. 2015.
[30] R. A. Lake and R. A. Coutu, "Using cross-linked SU-8 to flip-chip bond, assemble, and package MEMS devices," *IEEE Trans. Compon., Packag., Manuf. Technol.*, vol. 5, no. 3, pp. 301–306, Mar. 2015.
[31] *Diffusion Bonding*, accessed on Feb. 7, 2016. [Online]. Available: https://en.wikipedia.org/wiki/Diffusion_bonding
[32] Y. J. Cheng, W. Hong, and K. Wu, "94 GHz substrate integrated monopulse antenna array," *IEEE Trans. Antennas Propag.*, vol. 60, no. 1, pp. 121–129, Jan. 2012.
[33] S. Cheng, H. Yousef, and H. Kratz, "79 GHz slot antennas based on substrate integrated waveguides (SIW) in a flexible printed circuit board," *IEEE Trans. Antennas Propag.*, vol. 57, no. 1, pp. 64–71, Jan. 2009.
[34] D. Stephens, P. R. Young, and I. D. Robertson, "Millimeter-wave substrate integrated waveguides and filters in photoimageable thick-film technology," *IEEE Trans. Microw. Theory Techn.*, vol. 53, no. 12, pp. 3832–3838, Dec. 2005.
[35] A. Mahanfar, S.-W. Lee, A. M. Parameswaran, and R. G. Vaughan, "Self-assembled monopole antennas with arbitrary shapes and tilt angles for system-on-chip and system-in-package applications," *IEEE Trans. Antennas Propag.*, vol. 58, no. 9, pp. 3020–3028, Sep. 2010.
[36] M. F. Karim *et al.*, "Integration of SiP-based 60-GHz 4×4 Antenna array with CMOS OOK transmitter and LNA," *IEEE Trans. Microw. Theory Tech.*, vol. 59, no. 7, pp. 1869–1878, Jul. 2011.
[37] W. W. Hansen, "Radiating electromagnetic waveguide," U.S. Patent 2 402 622, Jun. 25, 1940.
[38] Y. Li, Q. Xue, E. K. N. Yung, and Y. Long, "The periodic half-width microstrip leaky-wave antenna with a backward to forward scanning capability," *IEEE Trans. Antennas Propag.*, vol. 58, no. 3, pp. 963–966, Mar. 2010.
[39] J. Liu, D. R. Jackson, and Y. Long, "Substrate integrated waveguide (SIW) leaky-wave antenna with transverse slots," *IEEE Trans. Antennas Propag.*, vol. 60, no. 1, pp. 20–29, Jan. 2012.
[40] N. K. Host, C.-C. Chen, J. L. Volakis, and F. A. Miranda, "Ku-band traveling wave slot array scanned via positioning a dielectric plunger," *IEEE Trans. Antennas Propag.*, vol. 63, no. 12, pp. 5475–5483, Dec. 2015.
[41] M. R. M. Hashemi and T. Itoh, "Evolution of composite right/left-handed leaky-wave antennas," *Proc. IEEE*, vol. 99, no. 10, pp. 1746–1754, Oct. 2011.
[42] D. R. Jackson, C. Caloz, and T. Itoh, "Leaky-wave antennas," *Proc. IEEE*, vol. 100, no. 7, pp. 2194–2206, Jul. 2012.
[43] *410 Series Waveguide to Coax Transition*, accessed on Jun. 2006. [Online]. Available: http://www.hi-technology.co.jp/japanese_folder/1-micro_folder/CTEC_Folder/PDF_Folder/MIWV-CATALOG.pdf
[44] W. Wang, S.-S. Zhong, Y.-M. Zhang, and X.-L. Liang, "A broadband slotted ridge waveguide antenna array," *IEEE Trans. Antennas Propag.*, vol. 54, no. 8, pp. 2416–2420, Aug. 2006.

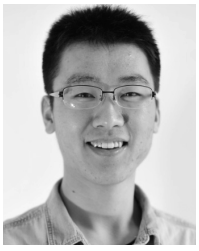

Le Chang (S'16) received the B.S. degree in electronics and information engineering from Xidian University, Xi'an, China, in 2012. He is currently pursuing the Ph.D. degree in electrical engineering at Tsinghua University, Beijing, China.

His current research interests include antenna design and theory, particularly in cavity antenna arrays, transmitted arrays, and millimeter-wave air-substrate antennas based on MEMS fabrication process.

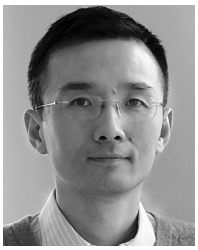

Zhijun Zhang (M'00–SM'04–F'15) received the B.S. and M.S. degrees from the University of Electronic Science and Technology of China, Chengdu, China, in 1992 and 1995, respectively, and the Ph.D. degree from Tsinghua University, Beijing, China, in 1999.

In 1999, he was a Post-Doctoral Fellow with the Department of Electrical Engineering, University of Utah, Salt Lake City, UT, USA, where he was appointed as a Research Assistant Professor in 2001. In 2002, he was an Assistant Researcher with the University of Hawaii at Manoa, Honolulu, HI, USA, and then joined Amphenol T & M Antennas, Vernon Hills, IL, USA, as a Senior Staff Antenna Development Engineer, and was later promoted to Antenna Engineer Manager. In 2004, he joined Nokia Inc., San Diego, CA, USA, as a Senior Antenna Design Engineer. In 2006, he joined Apple Inc., Cupertino, CA, USA, as a Senior Antenna Design Engineer and was then promoted to Principal Antenna Engineer. Since 2007, he has been with Tsinghua University, where he is currently a Professor with the Department of Electronic Engineering. He is the author of *Antenna Design for Mobile Devices* (Wiley, 2011).

Dr. Zhang was an Associate Editor of the IEEE TRANSACTIONS ON ANTENNAS AND PROPAGATION from 2010 to 2014 and the IEEE ANTENNAS AND WIRELESS PROPAGATION LETTERS from 2009 to 2015.

Yue Li (S'11–M'12) received the B.S. degree in telecommunication engineering from Zhejiang University, Zhejiang, China, in 2007, and the Ph.D. degree in electronic engineering from Tsinghua University, Beijing, China, in 2012.

He was a Visiting Scholar with the Institute for Infocomm Research, A*STAR, Singapore, in 2010, and a Principal Scholar of Tsinghua University in 2011, and the Hawaii Center of Advanced Communication, University of Hawaii at Manoa, Honolulu, HI, USA, in 2012. In 2012, he was a Post-Doctoral Fellow with the Department of Electronic Engineering, Tsinghua University. In 2013, he was a Research Scholar with the Department of Electrical and Systems Engineering, University of Pennsylvania, Philadelphia, PA, USA. Since 2016, he has been with Tsinghua University, where he is currently an Assistant Professor with the Department of Electronic Engineering. He has authored or coauthored 70 journal papers and over 30 international conference papers, and holds 14 granted Chinese patents. His current research interests include metamaterials, plasmonics, nanocircuits, electromagnetics, mobile and handset antennas, MIMO and diversity antennas, and millimeter-wave antennas and arrays.

Dr. Li was a recipient of the Young Scientist Award from URSI AP-RASC 2016, the Young Scientist Award from EMTS 2016, the Best Student Paper Award form ICMMT 2016, the Young Scientist Award from URSI General Assembly in 2014, and the Outstanding Doctoral Dissertation of Beijing in 2013.

Shaodong Wang, photograph and biography not available at the time of publication.

Zhenghe Feng (M'05–SM'08–F'12) received the B.S. degree in radio and electronics from Tsinghua University, Beijing, China, in 1970.

Since 1970, he has been with Tsinghua University as an Assistant, Lecturer, Associate Professor, and a Full Professor. His current research interests include numerical techniques and computational electromagnetics, RF and microwave circuits and antenna, wireless communications, smart antenna, and spatial temporal signal processing.